Bosons outperform fermions: The thermodynamic advantage of symmetry

Nathan M. Myers* and Sebastian Deffner†
Department of Physics, University of Maryland, Baltimore County, Baltimore, Maryland 21250, USA

(Received 14 October 2019; published 8 January 2020)

We examine a quantum Otto engine with a harmonic working medium consisting of two particles to explore the use of wave function symmetry as an accessible resource. It is shown that the bosonic system displays enhanced performance when compared to two independent single particle engines, while the fermionic system displays reduced performance. To this end, we explore the trade-off between efficiency and power output and the parameter regimes under which the system functions as engine, refrigerator, or heater. Remarkably, the bosonic system operates under a wider parameter space both when operating as an engine and as a refrigerator.

DOI: 10.1103/PhysRevE.101.012110

I. INTRODUCTION

With the widespread adoption of the steam engine during the industrial revolution, thermodynamics emerged as a physical theory that could describe and optimize the performance of these devices [1]. While modern thermodynamics has expanded far beyond its original scope, heat engines have remained the canonical systems for studying thermodynamic mechanisms. Not only do they have clear practical applications, but they also provide a paradigmatic way of studying how the thermodynamic properties of a system evolve—with applications ranging from biological processes, over climate systems, to black holes [2–4].

Quantum systems, subject to inherent fluctuations and decidedly nonequilibrium in nature, introduce new challenges for applying the framework of thermodynamics [5]. Nevertheless, quantum heat engines [5,6] provide a natural foundation for studying thermodynamic behavior in quantum systems in comprehensible terms. For instance, heat can always be found as the change in energy during an isochoric stroke, just as work can be found from the change in energy during an isentropic stroke [7].

This might explain the plethora of studies to investigate possible enhancements of engine performance through the exploitation of quantum resources including coherence [8–15], measurement effects [16], squeezed reservoirs [17–19], quantum phase transitions [20], and quantum many-body effects [15,21–23]. Other works have examined the fundamental differences between quantum and classical thermal machines [24–26], finite time cycles [13,27,28], utilizing shortcuts to adiabaticity [12,22,23,29–33], operating over nonthermal states [34,35], non-Markovian effects [36], magnetic systems [37–42], anharmonic potentials [43], optomechanical implementation [44], quantum dot implementation [38,40,42], implementation in 2D materials [38,41], classical engines coupled to quantum systems [45], quantum cooling [46,47], relativistic systems [48,49], degeneracy effects [39,50], and autonomous cycles [51]. Moreover, recent experimental advances have demonstrated the practical implementation of nanoscale heat engines [52,53], including those that harness quantum resources [54,55].

Two primary quantities of practical interest when characterizing the performance of a heat engine are its efficiency and power output. However, analysis of an ideal engine assumes that the strokes of the engine are carried out quasistatically over an infinitely slow period, maximizing efficiency but resulting in zero power output [7]. Rather, one is interested in the efficiency at maximum power (EMP) [56]. To this end, it has been shown that such analyses are particularly fruitful for quantum engines [19,57–65].

In this paper we explore a quantum Otto cycle similar to the model pioneered by Kosloff [57]. Our working medium consists of two particles in a harmonic trap. We examine performance, including efficiency, power, EMP, trade-off between efficiency and power, and the parameter regimes where the cycle functions as various types of thermal machines, depending on if the particles are bosons, fermions, or distinguishable (often referred to as "classical"). Through this, we explore the effect of wave function symmetry on engine performance. We find that in all examined performance characterizations the bosons perform better in comparison to the distinguishable particles, while the fermions perform worse. Symmetry effects in engine performance have been explored for other potentials or interactions [66–68]; however, our work provides additional insight through a fully analytical model of the complete dynamics, demonstrating how these effects arise solely from the underlying wave function symmetry.

II. PRELIMINARIES

Our working medium is given by two noninteracting, spinless particles, either both bosons or both fermions. Excluding any additional interaction terms and considering spinless particles (or alternatively particles of identical spin) allows us to isolate behavior arising from symmetry effects. The potential is a harmonic trap, such as a linear Paul trap, whose frequency can be varied with time. This is a two-particle generalization of the experimental system proposed in Ref. [65].

*myersn1@umbc.edu
†deffner@umbc.edu

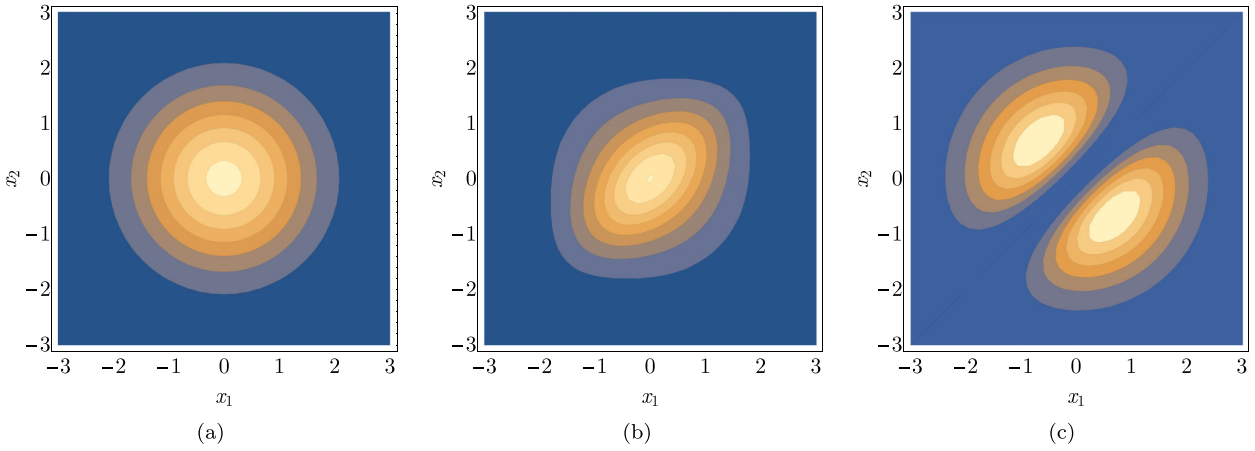

FIG. 1. Position distributions of the thermal state (7) of (a) two distinguishable particles, (b) two bosons, and (c) two fermions in a harmonic potential. Parameters are $\hbar = k_B = 1$ and $\beta = \omega = m = 1$.

To analyze an engine operating in finite time, we need the dynamics of a quantum harmonic oscillator with a time-dependent angular frequency $\omega(t)$ that varies from ω_1 at $t = 0$ to ω_2 at $t = \tau_s$. To this end, we start by briefly reviewing the case of a single particle, which we can then generalize to the case of two particles.

For a single particle the Hamiltonian is the sum of the kinetic and potential energies,

$$H = \frac{p^2}{2m} + \frac{1}{2}m\omega^2(t)x^2. \tag{1}$$

Following the method developed by Husimi [69] we can solve the time-dependent Schrödinger equation by introducing the Gaussian wave-function ansatz,

$$\psi_t(x) = \exp\left(\frac{i}{2\hbar}(a_t x^2 + 2b_t x + c_t)\right), \tag{2}$$

where a_t, b_t, and c_t are time-dependent coefficients. This allows us to reduce the Schrödinger equation to a set of three coupled differential equations for a_t, b_t, and c_t that can be solved by mapping to the equation of motion of the classical time-dependent harmonic oscillator,

$$\ddot{X}_t + \omega^2(t)X_t = 0. \tag{3}$$

The single-particle propagator then reads [69]

$$U_1 = \sqrt{\frac{m}{2\pi i\hbar X_t}}\exp\left(\frac{im}{2\hbar X_t}\left(\dot{X}_t x^2 - 2xx_0 + Y_t x_0^2\right)\right), \tag{4}$$

where X_t and Y_t are time-dependent solutions to Eq. (3) with initial conditions $X_0 = 0$, $\dot{X}_0 = 1$ and $Y_0 = 1$, $\dot{Y}_0 = 0$.

This framework can be directly expanded to two particles with Hamiltonian $H_{\mathrm{tot}} = H_1 + H_2$. For two particles the pure state wave function,

$$\Psi_{n_1,n_2}(x_1, x_2) = \tfrac{1}{2}\left[\psi_{n_1}(x_1)\psi_{n_2}(x_2) \pm \psi_{n_1}(x_2)\psi_{n_2}(x_1)\right], \tag{5}$$

consists of the symmetric (for bosons) or antisymmetric (for fermions) linear combination of the single particle wave functions.

Accordingly, the two-particle equilibrium thermal state reads

$$\rho_0(x_1, x_2, y_1, y_2) = \frac{1}{Z}\sum_{n_1=0}^{\infty}\sum_{n_2=0}^{\infty}\exp\left(-\beta\hbar\omega(n_1 + n_2 + 1)\right) \times \Psi^*_{n_1,n_2}(x_1, x_2)\Psi_{n_1,n_2}(y_1, y_2), \tag{6}$$

where Z is the standard partition function $Z = \mathrm{tr}\{\exp(-\beta H)\}$. Inserting the harmonic oscillator energy eigenstates in position representation for ψ_{n_1} and ψ_{n_2} yields the position space density operator,

$$\rho_0(x_1, x_2, y_1, y_2) = \frac{1}{Z}\frac{m\omega}{2\pi\hbar\,\sinh(\beta\hbar\omega)}\Big[e^{-\frac{m\omega}{4\hbar}\{[(x_1+y_1)^2+(x_2+y_2)^2]\tanh(\beta\hbar\omega/2)+[(x_1-y_1)^2+(x_2-y_2)^2]\coth(\beta\hbar\omega/2)\}} \pm e^{-\frac{m\omega}{4\hbar}\{[(x_2+y_1)^2+(x_1+y_2)^2]\tanh(\beta\hbar\omega/2)+[(x_2-y_1)^2+(x_1-y_2)^2]\coth(\beta\hbar\omega/2)\}}\Big]. \tag{7}$$

The thermal state (7) already displays notable differences in behavior arising from the wave function symmetry. This can be most easily observed from the states' Wigner quasiprobability distributions [70]. See Appendix B for the full expressions. By integrating the Wigner distributions over the momentum components we determine the position probability distributions for each thermal state. Figure 1 depicts the position distribution for two distinguishable particles, two bosons, and two fermions. The stretching of the boson distribution along the diagonal (where the position of the

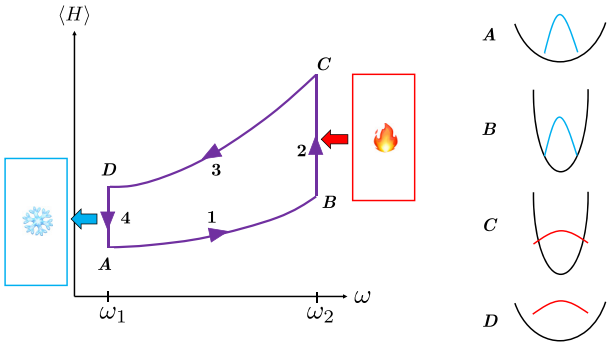

FIG. 2. Energy-frequency diagram of a quantum Otto cycle with representation of each stroke's trapping potential.

two particles coincide) is a demonstration of the effective attraction (boson bunching); conversely, the splitting of the fermion distribution along its diagonal is a demonstration of the corresponding effective repulsion between fermions (Pauli exclusion principle).

A heat engine cycle will necessarily involve some compression and expansion of the working medium. Considering this, the differences in the thermal state from the exchange forces already give us reason to suspect that symmetry should affect engine performance.

Finally, to determine the time evolved density operator we further require the proper two particle evolution operator. It can be shown that in energy representation the two particle propagator is the symmetric (for bosons) or antisymmetric (for fermions) linear combination of single particle propagators [71]. The same is true in position representation (see Appendix A for a full derivation),

$$U_2(x_1, x_1^0, x_2, x_2^0) = \tfrac{1}{2}\big[U_1(x_1, x_1^0)\,U_1(x_2, x_2^0) \pm U_1(x_1, x_2^0)\,U_1(x_2, x_1^0)\big], \tag{8}$$

where again the plus is for bosons and the minus for fermions.

III. FINITE-TIME QUANTUM OTTO CYCLE

Classically, the Otto cycle consists of four strokes: (1) isentropic compression, (2) isochoric heating, (3) isentropic expansion, and (4) isochoric cooling [7]. Note that the classical and the quantum Otto cycle are implemented in a fundamentally different manner: typically, in the quantum Otto cycle, the isentropic strokes are given by unitary strokes [5,57], such that the von Neumann entropy remains constant. This is in contrast to classical adiabatic strokes which are carried out quickly to prevent heat transference, and hence keep the thermodynamic entropy constant [7].

In our model the oscillator frequency plays the role of inverse volume, with the compression and expansion strokes corresponding to closing (increasing frequency) and opening the trap (decreasing frequency), respectively. The heating (cooling) stroke corresponds to coupling the oscillator respectively to a high (low) temperature bath that increases (decreases) the energy of the system [65]. This thermodynamic cycle is illustrated graphically in Fig. 2: at A the system is in an equilibrium thermal state with inverse temperature β_1 and frequency ω_1. The isentropic compression stroke is carried out via unitary evolution to nonthermal state B with increased frequency ω_2. The system is then coupled to the hot reservoir and allowed to thermalize to state C at inverse temperature β_2 and frequency ω_2. The frequency is then decreased unitarily during the expansion stroke resulting in state D with ω_1 and β_2. Finally, the system is coupled to the cold reservoir and allowed to thermalize back to β_1, returning it to its original state A.

Applying the two particle propagator derived above to the thermal state density operator we can determine the state of the system after either of the unitary strokes [(1) and (3)]. The full expression can be found in Appendix A. Using the explicit expression for the Wigner distribution of time evolved state (B4), we obtain the internal energy at each corner of the cycle,

$$\begin{aligned}
\langle H\rangle_A &= \frac{\hbar\omega_1}{2}[3\coth(\beta_1\hbar\omega_1) + \operatorname{csch}(\beta_1\hbar\omega_1) \mp 1],\\
\langle H\rangle_B &= \frac{\hbar\omega_2}{2}\,Q_{12}^*[3\coth(\beta_1\hbar\omega_1) + \operatorname{csch}(\beta_1\hbar\omega_1) \mp 1],\\
\langle H\rangle_C &= \frac{\hbar\omega_2}{2}[3\coth(\beta_2\hbar\omega_2) + \operatorname{csch}(\beta_2\hbar\omega_2) \mp 1],\\
\langle H\rangle_D &= \frac{\hbar\omega_1}{2}\,Q_{21}^*[3\coth(\beta_2\hbar\omega_2) + \operatorname{csch}(\beta_2\hbar\omega_2) \mp 1].
\end{aligned} \tag{9}$$

Here Q_{12}^* and Q_{21}^* are dimensionless parameters that measure the degree of adiabaticity of the isentropic strokes [69]. They are given by

$$Q^* = \frac{1}{2\omega_0\omega_{\tau_s}}\big[\omega_0^2\big(\omega_{\tau_s}^2 X_{\tau_s}^2 + \dot{X}_{\tau_s}^2\big) + \big(\omega_2^2 Y_{\tau_s}^2 + \dot{Y}_{\tau_s}^2\big)\big], \tag{10}$$

where X_t and Y_t are solutions of Eq. (3) with $\omega(t=0) = \omega_1$ and $\omega(t=\tau_s) = \omega_2$ during compression, and the reverse during the expansion. Note that for a completely adiabatic stroke $Q^* = 1$ and in general $Q^* \geqslant 1$ [65,69].

Since the only energy exchange during the isentropic strokes is in the form of work, we can determine the average work directly from the differences in internal energy $\langle W_1\rangle = \langle H\rangle_B - \langle H\rangle_A$ and $\langle W_3\rangle = \langle H\rangle_D - \langle H\rangle_C$. Analogously, we have from the isochoric strokes that $\langle Q_2\rangle = \langle H\rangle_C - \langle H\rangle_B$ and $\langle Q_4\rangle = \langle H\rangle_A - \langle H\rangle_D$.

IV. ENGINE CHARACTERIZATIONS

A. Efficiency and power

For any thermodynamic engine, the efficiency is defined as the ratio of the total work to the heat input while the power is defined by ratio of the total work to the cycle time,

$$\eta = -\frac{\langle W_1\rangle + \langle W_3\rangle}{\langle Q_2\rangle}, \quad P = \frac{\langle W_1\rangle + \langle W_3\rangle}{\tau}. \tag{11}$$

Thus the full two-particle efficiency becomes

$$\eta = 1 - Q_{21}^*\frac{\omega_1}{\omega_2} \mp \frac{\omega_1(Q_{12}^*Q_{21}^* - 1)[3\coth(\beta_1\hbar\omega_1) + \operatorname{csch}(\beta_1\hbar\omega_1) \mp 1]}{\omega_2\{\pm 3\coth(\beta_2\hbar\omega_2) \mp Q_{12}^*[3\coth(\beta_1\hbar\omega_1) + \operatorname{csch}(\beta_1\hbar\omega_1) \mp 1] \pm \operatorname{csch}(\beta_2\hbar\omega_2) - 1\}}, \tag{12}$$

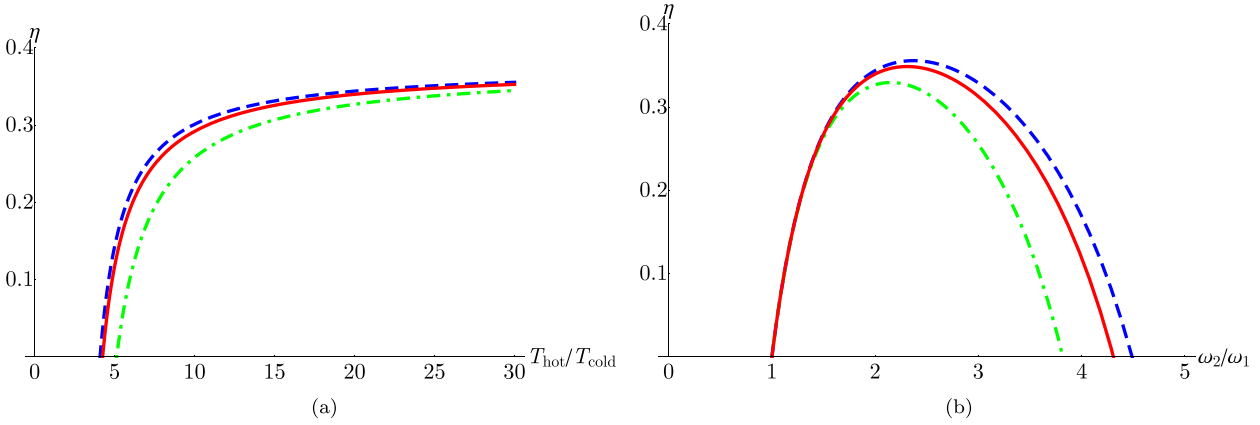

FIG. 3. Efficiency as a function of the ratio of bath temperatures (a) and final to initial frequencies (b) for a bosonic engine (dashed, blue line), fermionic engine (dot-dashed, green line), and single particle engine (solid, red line). We have taken $\hbar = k_B = 1$. Other parameters are for (a) $\omega_1 = 1$, $\omega_2 = 2$ and for (b) $T_{\rm cold} = 1$, $T_{\rm hot} = 20$.

where the top sign denotes the bosonic efficiency and the bottom sign the fermionic efficiency.

To check the consistency of our results, we examine the classical limit (high-temperature, quasistatic) of the maximum efficiency. In the quasistatic limit ($Q_{12}^* = Q_{21}^* = 1$) Eq. (12) reduces (as expected) to

$$\eta = 1 - \frac{\omega_1}{\omega_2}, \tag{13}$$

which is the quasistatic efficiency of the ideal quantum Otto engine [57].

In order to restrict the operation of our cycle to the regime in which it behaves as an engine (and thus ensure discussion of efficiencies is valid) we impose the following (positive work) conditions:

$$\langle Q_2 \rangle > 0, \quad \langle Q_4 \rangle < 0, \quad \langle W_{\rm total} \rangle > 0. \tag{14}$$

In the classical limit these positive work conditions are equivalent to

$$\frac{\beta_2}{\beta_1} \leqslant \frac{\omega_1}{\omega_2}. \tag{15}$$

Therefore, we see that, indeed, the maximum efficiency becomes

$$\eta_{\rm max} = 1 - \frac{T_c}{T_h}, \tag{16}$$

which is just the Carnot efficiency.

To examine the behavior of the efficiency and power outside of limiting cases we first select a protocol $\omega(t)$. For the sake of simplicity, we start with the "sudden switch" protocol, which corresponds to an instantaneous change from ω_1 to ω_2 [65]. In this case

$$Q_{12}^* = Q_{21}^* = \frac{\omega_2^2 + \omega_1^2}{2\omega_2\omega_1}. \tag{17}$$

The efficiency for bosonic and fermionic engines using this protocol is shown in comparison to that of a single particle quantum Otto engine in Fig. 3. Note that efficiency is identical for the sum of any number of single particle engines. We see a notable enhancement in efficiency over the single particle engine at intermediate bath temperature ratios for the bosonic engine, and a universal decrease in efficiency for the fermionic engine. We see a similar enhancement for bosons and reduction for fermions at high frequency ratios.

The power output for bosonic and fermionic engines using this protocol is shown in comparison to that of the sum of two, macroscopically distinguishable single particle quantum Otto engines in Fig. 4. Note that in the case of the sudden switch protocol the cycle time, τ, consists of just the sum of the thermalization times, as the isentropic strokes are considered to be instantaneous. A direct calculation of the thermalization time requires an explicit model of the bath-system interaction, which is beyond the scope of this paper. In order to estimate the power, we have taken $\tau = 1$, leaving optimization of power with respect to cycle time as a topic for future work. Again, we see an enhancement to the power output in the case of bosons, and a significantly larger decrease in power output in the case of fermions, in comparison to the equivalent number of distinguishable single particle engines.

B. Efficiency at maximum power

As stated above, due to the inherent trade-off between efficiency and power, the more practically significant characterization of heat engine performance is the efficiency at maximum power. To determine this, we first maximize the power with respect to the second frequency, ω_2, assuming ω_1, the cycle time, and the bath temperatures are held fixed.

Carrying out this maximization in the classical limit yields

$$\frac{\omega_2}{\omega_1} = \sqrt{\frac{\beta_1}{\beta_2}}. \tag{18}$$

Thus we have

$$\eta_{\rm EMP} = 1 - \sqrt{\frac{T_c}{T_h}}, \tag{19}$$

which is nothing else but the Curzon-Ahlborn efficiency [56]. This is in full agreement with recent findings in Refs. [61]

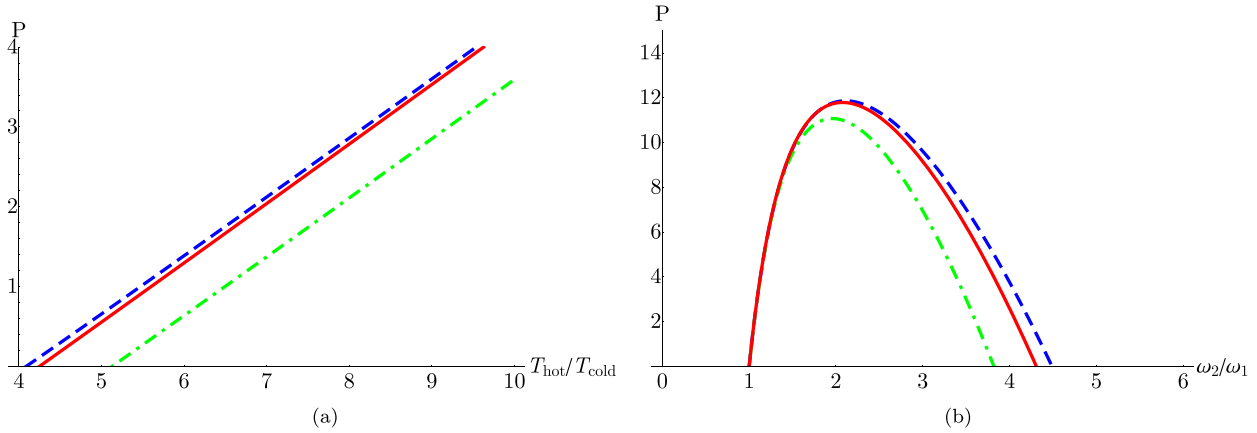

FIG. 4. Power as a function of the ratio of bath temperatures (a) and final to initial frequencies (b) for a bosonic engine (dashed, blue line), fermionic engine (dot-dashed, green line), and two distinguishable single particle engines (solid, red line). We have taken $\hbar = k_B = 1$. Other parameters are for (a) $\omega_1 = 1$, $\omega_2 = 2$, $\tau = 1$ and for (b) $T_{\rm cold} = 1$, $T_{\rm hot} = 20$, $\tau = 1$.

and [63] that show in the quasistatic and classical high-temperature limits, respectively, the EMP of a quantum harmonic Otto is given by Eq. (19).

To examine the EMP outside of the classical limit we again choose the sudden switch protocol. Figure 5 shows the EMP as a function of the ratio of bath temperatures for our three working mediums. Here we see the same pattern as before, an enhancement over the equivalent number of single particle engines in the case of bosons, and a significantly larger reduction in the case of fermions.

C. Efficiency and power trade-off

While the EMP provides information about the amount of efficiency sacrificed to achieve *maximum* power, it can be enlightening to also examine the trade-off across the entire parameter space. Various trade-off measures have been put forward (see Refs. [72–79] for further discussion). Here we use the "efficient power" criterion proposed by Yilmaz, which is defined as the simple product of efficiency and power [75]. This provides us with a direct measure of the power output gained per corresponding unit decrease in efficiency. The difference in efficient power between the bosons and fermions for the case of the sudden switch protocol is shown in Fig. 6 as a function of both the ratio of bath temperatures and initial and final frequencies. We see that over the whole parameter space the efficient power for bosons is superior to the trade-off for fermions.

D. Operational parameter regimes

Aside from engine characterizations, the other main area in which a quantum advantage could manifest is in the size of the parameter space in which the cycle functions as the desired type of thermal machine. In general, there are four possible types of thermal machines allowed by the second law: engine, refrigerator, and two types of heater [80]. An engine extracts

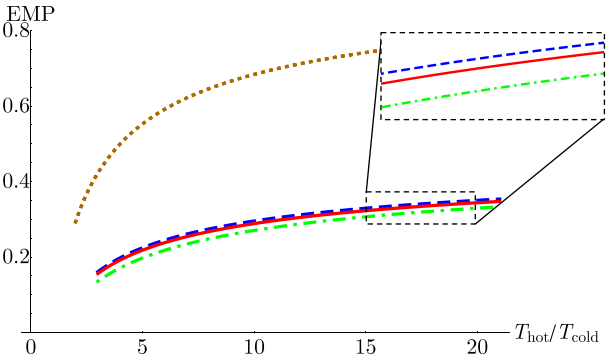

FIG. 5. EMP as a function of the ratio of bath temperatures for a bosonic engine (dashed, blue line), fermionic engine (dot-dashed, green line), and two distinguishable single particle engines (solid, red line) given in comparison to the Curzon-Ahlborn efficiency (dotted, brown line). We have taken $\hbar = k_B = 1$. Other parameters are $\omega_1 = 1$ and $\tau = 1$.

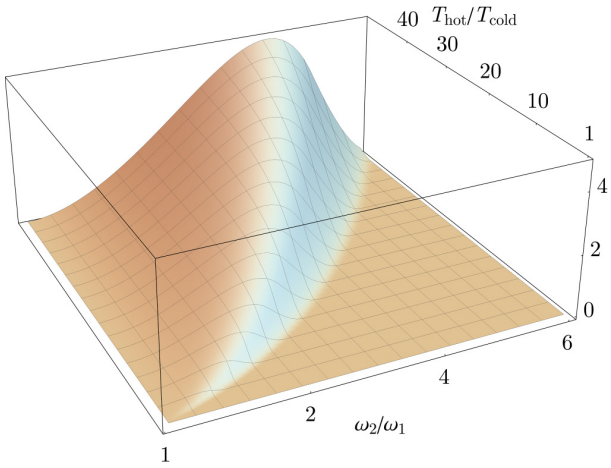

FIG. 6. Difference between bosonic and fermionic efficient power as a function of the ratio of both bath temperatures and initial and final frequencies. We have taken $\hbar = k_B = 1$ and $\tau = 1$.

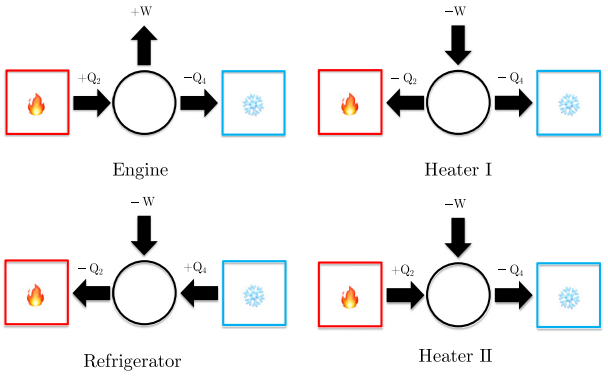

FIG. 7. Block diagrams for all allowed thermal machines.

work from heat flowing between a hot and cold reservoir. A refrigerator puts in work in order to facilitate the flow of heat from a cold to a hot reservoir. The first type of heater puts in work that is then dissipated as heat into both reservoirs. The second type of heater puts in work to facilitate the flow of heat from the hot to the cold reservoir. The operation of these machines is summarized in Fig. 7.

When thinking practically, heater II is clearly the least desired mode of operation as it involves spending work to facilitate a process that will occur spontaneously. With this in mind we define an advantage as an expansion of the parameter space under which the cycle functions as either engine, refrigerator, or heater I and a corresponding reduction in the parameter space where it functions as heater II.

By determining the signs for the work and heat components we can determine which thermal machine the cycle is functioning as for any combination of frequencies and bath temperatures. Figure 8 gives a comparison between the operational space of the bosonic, fermionic, and distinguishable particle systems as a function of their parameters. We see that the bosonic system experiences an expanded operational space for both the engine, refrigerator, and heater I machines in comparison to both fermions [Fig. 8(a)] and an equivalent number of distinguishable single particle engines [Fig. 8(b)]. Conversely the fermionic system experiences a reduced operational space under the same comparisons [Fig. 8(a) and Fig. 8(c)]. This demonstrates a clear advantage for the bosonic engine by our above definition.

E. Linear protocol and instantaneous power

It is also of interest to explore how the operational spaces evolve as the cycle transitions from the instantaneous sudden switch protocol to the infinite-time quasistatic limit. In order to do so we consider a linear protocol that allows us to interpolate smoothly between these limits,

$$\omega(t) = \left(\omega_1^2 + \delta\omega \frac{t}{\tau_s}\right)^{1/2}, \tag{20}$$

where τ_s is the duration of the isentropic strokes. A comparison between the the operational space of the bosonic and fermionic systems at selected stroke durations is shown in Fig. 9. As stroke duration increases the heater I and heater II regimes shrink while the engine and refrigerator regimes expand. We see for very large τ_s, i.e., approximately quasistatic, the heater regimes disappear entirely and the boson and fermion operational diagrams become nearly identical. This matches expectations as the heaters are fundamentally nonequilibrium machines. The convergence of the operational diagrams is due to the fact that in the quasistatic limit both cycles' performance approach the same limits (such as the Carnot and Curzon-Ahlborn efficiencies).

In conclusion, we have seen in all explored characteristics that the bosonic working medium outperforms the fermionic one. The linear protocol allows us to examine how the internal energy and power evolve throughout the isentropic strokes which can provide us with insight into the source of this advantage.

Figure 10 depicts the instantaneous power (the time derivative of the instantaneous internal energy) during both the expansion (opening) and compression (closing) strokes. We see that at any given time during the expansion stroke the bosons are *extracting* less work than an equivalent number of distinguishable single particle engines, but at the same time during the compression stroke they require less work *input* resulting in a net gain in performance. The reverse is true for fermions. However, in their case the extra work input required

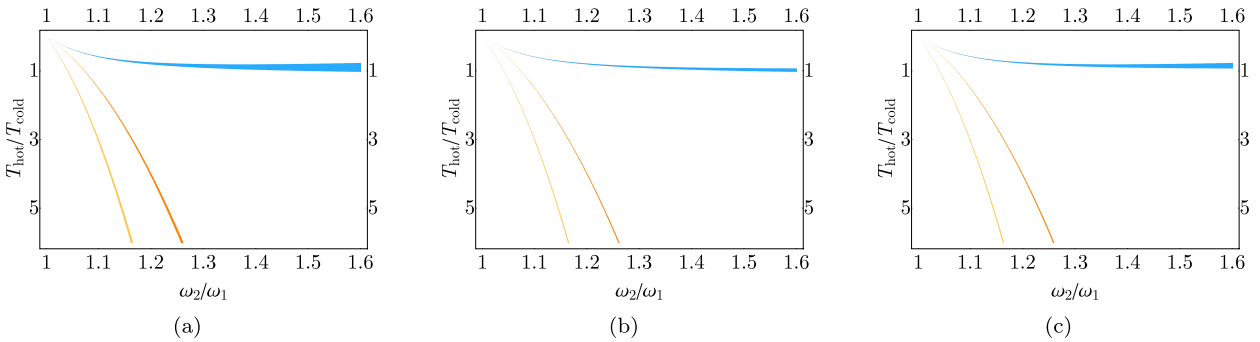

FIG. 8. Operational diagrams whose shaded portions give the regions in parameter space under which the cycle functions as an engine (bottom, yellow region), heater I (middle, orange region), and refrigerator (top, blue region) for one working medium, but not for the compared medium. Panel (a) compares bosons and fermions, (b) compares bosons and distinguishable single particles, and (c) compares distinguishable single particles and fermions. Parameters are $\hbar = k_B = 1$.

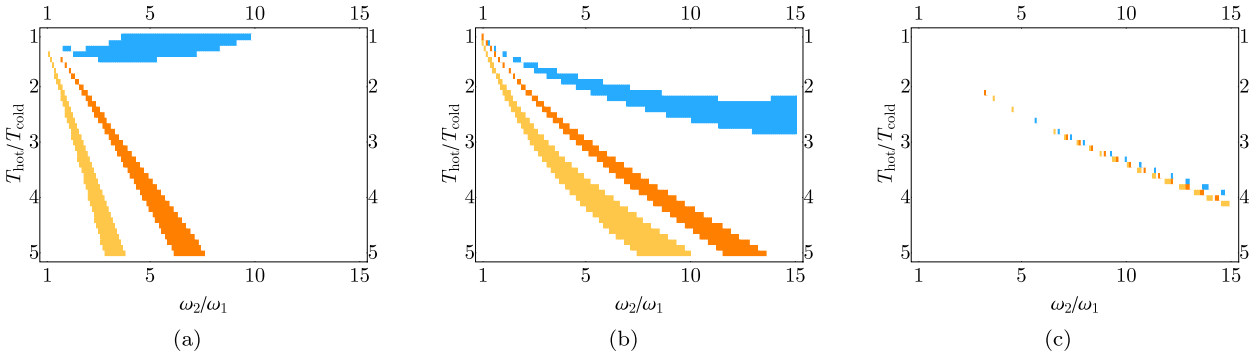

FIG. 9. Operational diagrams whose shaded portions give the regions in parameter space under which the cycle functions as an engine (bottom, yellow region), heater I (middle, orange region), and refrigerator (top, blue region) for bosons, but not for fermions. We have taken the linear protocol with stroke durations (a) $\tau_s = 1$, (b) $\tau_s = 10$, and (c) $\tau_s = 200$. Parameters are $\hbar = k_B = 1$.

outweighs the advantage they gain on extraction resulting in a net decrease in performance. Physically, this means that the repulsive force between fermions hinders more on compression than it aids in expansion, while the opposite is true of the attractive force between bosons. We also note that the slope of the instantaneous power and the separation between each case remains roughly constant (aside from some small oscillations induced by the form of Q^* in the linear protocol). This is an indication that the variation in performance arises solely from the differences in internal energy and not from differences in entropy induced by changes in quantum correlations.

V. CONCLUDING REMARKS

In this work we have examined a quantum Otto engine operating on a two-particle working medium consisting of either spinless bosons or fermions through fully analytical models of the state dynamics. We have shown that in all examined engine characterizations, including efficiency, power, EMP, trade-off between efficiency and power, and operational parameter space, the bosonic system displays enhanced performance while the fermionic system displays reduced performance. This enhancement (or reduction) persists in comparison to the performance of an equivalent number of distinguishable single-particle quantum engines clearly indicating that this effect arises from the particle symmetry. We have examined the time-dependent behavior of the instantaneous power output throughout the isentropic strokes for the case of a linear protocol and found that the origin of this effect lies in the differences in internal energy between the bosons and fermions that result from the Pauli exclusion principle. While the displayed advantage is moderate, we believe protocols can be developed that optimize this resource for more significant enhancement to performance. However, the development and analysis of such protocols is beyond the scope of this work.

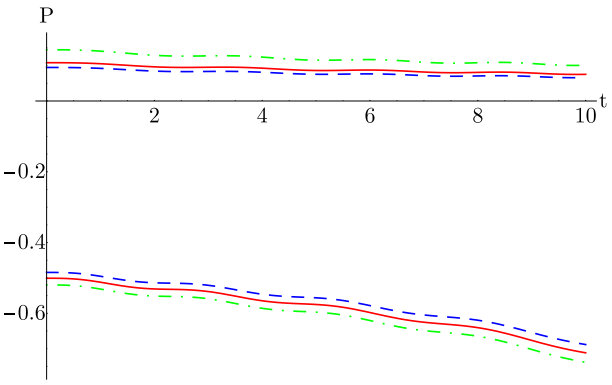

FIG. 10. Instantaneous power output during the compression (positive-valued lines) and expansion (negative-valued lines) strokes for bosons (dashed, blue line), fermions (dot-dashed, green line), and the sum of two distinguishable single particle engines (solid, red line). Note that in this case negative power represents work *extraction* from the engine. We have taken $\hbar = k_B = 1$. Other parameters are $\omega_1 = 1$, $\omega_2 = \sqrt{2}$, $\tau = 10$, $T_{\rm cold} = 1$, and $T_{\rm hot} = 10$.

Wave-function symmetry is an inherently quantum property; as such, this increase in performance (for bosons) is a demonstration of a truly quantum advantage. Beyond this, however, the wave-function symmetry is also an additional *information-bearing degree of freedom* [81] available to the system. Using information as a resource in a thermodynamic system is an area that has seen much recent activity [82–94]. We leave an examination of how this additional information resource may be leveraged, along with the effects of interparticle interactions [95,96] and scalability, as topics to be explored in future work.

ACKNOWLEDGMENTS

It is a pleasure to thank Priyo Shankar Pal for informative discussion, especially in regards to the operational characterization of nonequilibrium thermal machines, as well as Akram Touil for enlightening conversation in regards to information measures in thermodynamic systems. S.D. acknowledges support from the US National Science Foundation under Grant No. CHE-1648973. This research was supported by Grant No. FQXi-RFP-1808 from the Foundational Questions Institute and Fetzer Franklin Fund, a donor advised fund of Silicon Valley Community Foundation (S.D.).

APPENDIX A: TWO PARTICLE PROPAGATOR

In this Appendix we outline the derivation of the propagator in space representation for a two particle harmonic system and apply it to the thermal state density operator. For a given two particle state represented by density operator ρ the propagator is defined by

$$\rho_t(x_1,x_2,y_1,y_2)=\int dx_1^0\int dx_2^0\int dy_1^0\int dy_2^0\,U_2\big(x_1,x_1^0,x_2,x_2^0\big)\rho_0\big(x_1^0,x_2^0,y_1^0,y_2^0\big)U_2^\dagger\big(y_1,y_1^0,y_2,y_2^0\big). \tag{A1}$$

Note that in energy representation [71]

$$\langle n_1n_2|U_2\big|n_1^0n_2^0\rangle=\tfrac{1}{2}\big[\langle n_1|U_1\big|n_1^0\rangle\langle n_2|U_1\big|n_2^0\rangle\pm\langle n_1|U_1\big|n_2^0\rangle\langle n_2|U_1\big|n_1^0\rangle\big]. \tag{A2}$$

Changing the basis in the expression (A1) into energy representation and comparing terms, we have

$$U_2=\frac{1}{2}\sum_{n_1,n_2=0}^{\infty}\langle x_1x_2|n_1n_2\rangle\left[\sum_{n_1^0,n_2^0=0}^{\infty}\big(\langle n_1|U_1\big|n_1^0\rangle\langle n_2|U_1\big|n_2^0\rangle\pm\big\langle n_1|U_1\big|n_2^0\big\rangle\langle n_2|U_1\big|n_1^0\rangle\big)\langle n_1^0n_2^0|x_1^0x_2^0\rangle\right], \tag{A3}$$

where

$$\langle x_1x_2|n_1n_2\rangle=\tfrac{1}{2}[\psi_{n_1}(x_1)\psi_{n_2}(x_2)\pm\psi_{n_1}(x_2)\psi_{n_2}(x_1)]. \tag{A4}$$

Further in position representation the harmonic oscillator energy eigenstates are

$$\psi_n(x)=\frac{1}{\sqrt{2^nn!}}\left(\frac{m\omega}{\pi\hbar}\right)^{1/4}e^{-\frac{m\omega x^2}{2\hbar}}H_n\left(\sqrt{\frac{m\omega}{\hbar}}x\right), \tag{A5}$$

and the orthogonality condition of the Hermite polynomials is

$$\sum_{n=0}^{\infty}\frac{1}{\sqrt{2^nn!}}H_n(x)H_n(y)=\sqrt{\pi}e^{\frac{1}{2}(x^2+y^2)}\delta(x-y), \tag{A6}$$

where $\delta(x-y)$ is the Dirac delta. Thus we obtain

$$U_2\big(x_1,x_1^0,x_2,x_2^0\big)=\tfrac{1}{2}\big[U_1\big(x_1,x_1^0\big)U_1\big(x_2,x_2^0\big)\pm U_1\big(x_1,x_2^0\big)U_1\big(x_2,x_1^0\big)\big], \tag{A7}$$

with the same method allowing for the simplification of the conjugate to a similar expression.

Applying the two particle propagator to the thermal state (7) yields the full time-evolved density operator,

$$\begin{aligned}\rho_t(x_1,x_2,y_1,y_2)=&\frac{m\omega}{2\pi\hbar(Y_t^2+X_t^2\omega^2)}\big(e^{\mp\beta\hbar\omega}-1\big)\\&\times\Big\{e^{\frac{m}{2\hbar(Y_t^2+X_t^2\omega^2)}[i(x_1^2+x_2^2-y_1^2-y_2^2)(Y_t\dot{Y}_t+X_t\dot{X}_t\omega^2)-\omega(x_1^2+x_2^2+y_1^2+y_2^2)\coth(\beta\hbar\omega)+2\omega(x_1y_1+x_2y_2)\operatorname{csch}(\beta\hbar\omega)]}\\&\pm e^{\frac{m}{2\hbar(Y_t^2+X_t^2\omega^2)}[i(x_1^2+x_2^2-y_1^2-y_2^2)(Y_t\dot{Y}_t+X_t\dot{X}_t\omega^2)-\omega(x_1^2+x_2^2+y_1^2+y_2^2)\coth(\beta\hbar\omega)+2\omega(x_2y_1+x_1y_2)\operatorname{csch}(\beta\hbar\omega)]}\Big\}.\end{aligned} \tag{A8}$$

Here the top sign denotes the boson state and the bottom sign denotes the fermion state.

APPENDIX B: WIGNER FORMALISM

Finally, we outline the derivation of the thermal and time-evolved state Wigner distributions. The definition of the Wigner distribution generalized to a two particle density matrix is

$$W(x_1,p_1,x_2,p_2)=\frac{1}{4\pi^2\hbar^2}\int du_1\int du_2\,\rho\Big(x_1+\frac{u_1}{2},x_2+\frac{u_2}{2},x_1-\frac{u_1}{2},x_2-\frac{u_2}{2}\Big)e^{-\frac{ip_1u_1}{\hbar}}e^{-\frac{ip_2u_2}{\hbar}}. \tag{B1}$$

Plugging in the thermal state we obtain the thermal state Wigner function,

$$\begin{aligned}W_0(x_1,p_1,x_2,p_2)=&\frac{\operatorname{sech}^2(\beta\hbar\omega/2)}{\pi^2\hbar^2[\operatorname{csch}^2(\beta\hbar\omega/2)\pm2\operatorname{csch}(\beta\hbar\omega)]}\\&\times\Big(e^{-\frac{[p_1^2+p_2^2+m^2(x_1^2+x_2^2)\omega^2]\tanh(\beta\hbar\omega/2)}{m\omega\hbar}}\pm2\,e^{\frac{-[p_1^2+p_2^2+m^2(x_1^2+x_2^2)\omega^2]\coth(\beta\hbar\omega)+2(p_1p_2+m^2\omega^2x_1x_2)\operatorname{csch}(\beta\hbar\omega)}{m\omega\hbar}}\Big).\end{aligned} \tag{B2}$$

Here the top sign denotes the boson distribution and the bottom sign the fermion. Integrating over the momentum coordinates yields the position-space probability distribution, plotted in Fig. 1,

$$\begin{aligned}P_x(x_1,x_2)=&\frac{2m\omega}{\pi\hbar}\frac{\operatorname{csch}(\beta\hbar\omega)}{\operatorname{csch}^2(\beta\hbar\omega/2)\pm2\operatorname{csch}(\beta\hbar\omega)}\\&\times\Big(e^{-\frac{m\omega}{\hbar}(x_1^2+x_2^2)\tanh(\beta\hbar\omega/2)}\pm e^{-\frac{m\omega}{\hbar}[-2x_1x_2+(x_1^2+x_2^2)\cosh(\beta\hbar\omega)]\operatorname{csch}(\beta\hbar\omega)}\Big).\end{aligned} \tag{B3}$$

Repeating the same process for the time-evolved density operator, given in (9), yields the time-evolved Wigner distribution,

$$W_t(x_1, p_1, x_2, p_2) = \frac{1}{2\pi^2\hbar^2}\Big[e^{-\frac{[p_1^2\alpha^2+p_2^2\alpha^2-2m\alpha\gamma(p_1x_1+p_2x_2)+m^2(x_1^2+x_2^2)(\omega^2+\gamma^2)]\tanh[\frac{1}{2}\beta\hbar\omega]}{\alpha m\omega\hbar}}(\pm 1 \mp e^{\mp\beta\hbar\omega})\tanh(\beta\hbar\omega/2)$$
$$\mp e^{-\frac{\coth(\beta\hbar\omega)(p_1^2\alpha^2+p_2^2\alpha^2-2m\alpha\gamma(p_1x_1+p_2x_2)+m^2(x_1^2+x_2^2)(\omega^2+\gamma^2)-2\{p_1\alpha[Y_t(p_2Y_t-mx_2\dot{Y}_t)+X_t(p_2X_t-mx_2\dot{X}_t)\omega^2]+mx_1[-p_2\alpha\gamma+mx_2(\omega^2+\gamma^2)]\}\mathrm{sech}(\beta\hbar\omega))}{\alpha m\omega\hbar}}$$
$$\times (\mp 1 \pm e^{\mp\beta\hbar\omega})\Big], \tag{B4}$$

where $\alpha = Y_t^2 + X_t^2\omega^2$ and $\gamma = Y_t\dot{Y}_t + X_t\dot{X}_t\omega^2$.

[1] D. Kondepudi and I. Prigogine, *Modern Thermodynamics* (Wiley, New York, 1998).

[2] A. W. J. Muller, Thermoelectric energy conversion could be an energy source of living organisms, Phys. Lett. A **96**, 319 (1983).

[3] N. Shaw, *Manual of Meteorology: Volume III* (Cambridge University Press, London, 1919).

[4] C. V. Johnson, Holographic heat engines, Class. Quantum Grav. **31**, 205002 (2014).

[5] S. Deffner and S. Campbell, *Quantum Thermodynamics* (Morgan and Claypool, Bristol, 2019).

[6] H. E. D. Scovil and E. O. Schulz-DuBois, Three-Level Masers as Heat Engines, Phys. Rev. Lett. **2**, 262 (1959).

[7] H. B. Callen, *Thermodynamics and an Introduction to Thermostatistics* (Wiley, New York, 1985).

[8] M. O. Scully, M. S. Zubairy, G. S. Agarwal, and H. Walther, Extracting work from a single heat bath via vanishing quantum coherence, Science **299**, 862 (2003).

[9] M. O. Scully, K. R. Chapin, K. E. Dorfman, M. B. Kim, and A. Svidzinsky, Quantum heat engine power can be increased by noise-induced coherence, Proc. Natl. Acad. Sci. U.S.A. **108**, 15097 (2011).

[10] R. Uzdin, Coherence-induced reversibility and collective operation of quantum heat machines via coherence recycling, Phys. Rev. Appl. **6**, 024004 (2016).

[11] G. Watanabe, B. P. Venkatesh, P. Talkner, and A. del Campo, Quantum Performance of Thermal Machines Over Many Cycles, Phys. Rev. Lett. **118**, 050601 (2017).

[12] R. Dann and R. Kosloff, Quantum signatures in the quantum Carnot cycle, arXiv:1906.06946.

[13] T. Feldmann and R. Kosloff, Short time cycles of purely quantum refrigerators, Phys. Rev. E **85**, 051114 (2012).

[14] G. Watanabe, B. P. Venkatesh, P. Talkner, M. J. Hwang, and A. del Campo, Quantum statistical enhancement of the collective performance of multiple bosonic engines, arXiv:1904.07811.

[15] A. U. C. Hardal and O. E. Müstecaplioglu, Superradiant quantum heat engine, Sci. Rep. **5**, 12953 (2015).

[16] L. Buffoni, A. Solfanelli, P. Verrucchi, A. Cuccoli, and M. Campisi, Quantum Measurement Cooling, Phys. Rev. Lett. **122**, 070603 (2019).

[17] W. Niedenzu, V. Mukherjee, A. Ghosh, A. G. Kofman, and G. Kurizki, Quantum engine efficiency bound beyond the second law of thermodynamics, Nat. Commun. **9**, 165 (2018).

[18] R. Long and W. Liu, Performance of quantum Otto refrigerators with squeezing, Phys. Rev. E **91**, 062137 (2015).

[19] J. Roßnagel, O. Abah, F. Schmidt-Kaler, K. Singer, and E. Lutz, Nanoscale Heat Engine Beyond the Carnot Limit, Phys. Rev. Lett. **112**, 030602 (2014).

[20] Y. H. Ma, S. H. Su, and C. P. Sun, Quantum thermodynamic cycle with quantum phase transition, Phys. Rev. E **96**, 022143 (2017).

[21] Y. Y. Chen, G. Watanabe, Y. C. Yu, X. W. Guan, and A. del Campo, An interaction-driven many-particle quantum heat engine and its universal behavior, Npj Quantum Inf. **5**, 88 (2019).

[22] M. Beau, J. Jaramillo, and A. del Campo, Scaling-up quantum heat engines efficiently via shortcuts to adiabaticity, Entropy **18**, 168 (2016).

[23] J. Li, T. Fogarty, S. Campbell, X. Chen, and T. Busch, An efficient nonlinear Feshbach engine, New J. Phys. **20**, 015005 (2018).

[24] H. T. Quan, Y.-x. Liu, C. P. Sun, and F. Nori, Quantum thermodynamic cycles and quantum heat engines, Phys. Rev. E **76**, 031105 (2007).

[25] B. Gardas and S. Deffner, Thermodynamic universality of quantum Carnot engines, Phys. Rev. E **92**, 042126 (2015).

[26] A. Friedenberger and E. Lutz, When is a quantum heat engine quantum? Europhys. Lett. **120**, 10002 (2017).

[27] V. Cavina, A. Mari, and V. Giovannetti, Slow Dynamics and Thermodynamics of Open Quantum Systems, Phys. Rev. Lett. **119**, 050601 (2017).

[28] Y. Zheng, P. Hänggi, and D. Poletti, Occurrence of discontinuities in the performance of finite-time quantum Otto cycles, Phys. Rev. E **94**, 012137 (2016).

[29] O. Abah and E. Lutz, Performance of shortcut-to-adiabaticity quantum engines, Phys. Rev. E **98**, 032121 (2018).

[30] O. Abah and M. Paternostro, Shortcut-to-adiabaticity Otto engine: A twist to finite-time thermodynamics, Phys. Rev. E **99**, 022110 (2019).

[31] O. Abah and E. Lutz, Energy efficient quantum machines, Europhys. Lett. **118**, 40005 (2017).

[32] A. del Campo, J. Goold, and M. Paternostro, More bang for your buck: Super-adiabatic quantum engines, Sci. Rep. **4**, 6208 (2014).

[33] K. Funo, N. Lambert, B. Karimi, J. P. Pekola, Y. Masuyama, and F. Nori, Speeding up a quantum refrigerator via counterdiabatic driving, Phys. Rev. B **100**, 035407 (2019).

[34] N. Yunger Halpern, C. D. White, S. Gopalakrishnan, and G. Refael, Quantum engine based on many-body localization, Phys. Rev. B **99**, 024203 (2019).

[35] C. Cherubim, F. Brito, and S. Deffner, Non-thermal quantum engine in transmon qubits, Entropy **21**, 545 (2019).

[36] R. Uzdin, A. Levy, and R. Kosloff, Quantum heat machines equivalence, work extraction beyond Markovianity, and strong coupling via heat exchangers, Entropy **18**, 124 (2016).

[37] E. Muñoz and F. J. Peña, Magnetically driven quantum heat engine, Phys. Rev. E **89**, 052107 (2014).

[38] E. Muñoz, F. J. Peña, and A. González, Magnetically-driven quantum heat engines: The quasi-static limit of their efficiency, Entropy **18**, 173 (2016).

[39] F. J. Peña, A. González, A. Nunez, P. Orellana, R. Rojas, and P. Vargas, Magnetic engine for the single-particle Landau problem, Entropy **19**, 639 (2017).

[40] F. J. Peña, O. Negrete, G. Alvarado Barrios, D. Zambrano, A. González, A. S. Nunez, P. A. Orellana, and P. Vargas, Magnetic Otto engine for an electron in a quantum dot: Classical and quantum approach, Entropy **21**, 512 (2019).

[41] F. J. Peña, D. Zambrano, O. Negrete, G. De Chiara, P. A. Orellana, and P. Vargas, Quantum and classical Otto engine for a 2-d material: the case of a graphene quantum dot, arXiv:1909.08694.

[42] F. J. Peña and E. Muñoz, Magnetostrain-driven quantum engine on a graphene flake, Phys. Rev. E **91**, 052152 (2015).

[43] Y. Zheng and D. Poletti, Work and efficiency of quantum Otto cycles in power-law trapping potentials, Phys. Rev. E **90**, 012145 (2014).

[44] K. Zhang, F. Bariani, and P. Meystre, Quantum Optomechanical Heat Engine, Phys. Rev. Lett. **112**, 150602 (2014).

[45] M. O. Scully, Quantum Afterburner: Improving the Efficiency of an Ideal Heat Engine, Phys. Rev. Lett. **88**, 050602 (2002).

[46] A. Levy and R. Kosloff, Quantum Absorption Refrigerator, Phys. Rev. Lett. **108**, 070604 (2012).

[47] W. Niedenzu, I. Mazets, G. Kurizki, and F. Jendrzejewski, Quantized refrigerator for an atomic cloud, Quantum **3**, 155 (2019).

[48] F. J. Peña, M. Ferré, P. A. Orellana, R. G. Rojas, and P. Vargas, Optimization of a relativistic quantum mechanical engine, Phys. Rev. E **94**, 022109 (2016).

[49] E. Muñoz and F. J. Peña, Quantum heat engine in the relativistic limit: The case of a Dirac particle, Phys. Rev. E **86**, 061108 (2012).

[50] G. Barrios, F. J. Peña, F. Albarrán-Arriagada, P. Vargas, and J. Retamal, Quantum mechanical engine for the quantum Rabi model, Entropy **20**, 767 (2018).

[51] A. Roulet, S. Nimmrichter, and J. M. Taylor, An autonomous single-piston engine with a quantum rotor, Quantum Sci. Technol. **3**, 035008 (2018).

[52] J. Roßnagel, S. T. Dawkins, K. N. Tolazzi, O. Abah, E. Lutz, F. Schmidt-Kaler, and K. Singer, A single-atom heat engine, Science **352**, 325 (2016).

[53] M. Josefsson, A. Svilans, A. M. Burke, E. A. Hoffmann, S. Fahlvik, C. Thelander, M. Leijnse, and H. Linke, A quantum-dot heat engine operating close to the thermodynamic efficiency limits, Nat. Nanotechnol. **13**, 920 (2018).

[54] J. Klaers, S. Faelt, A. Imamoglu, and E. Togan, Squeezed Thermal Reservoirs as a Resource for a Nanomechanical Engine Beyond the Carnot Limit, Phys. Rev. X **7**, 031044 (2017).

[55] N. Van Horne, D. Yum, T. Dutta, P. Hänggi, J. Gong, D. Poletti, and M. Mukherjee, Single atom energy-conversion device with a quantum load, arXiv:1812.01303.

[56] F. L. Curzon and B. Ahlborn, Efficiency of a Carnot engine at maximum power output, Am. J. Phys. **43**, 22 (1975).

[57] R. Kosloff, A quantum mechanical open system as a model of a heat engine, J. Chem. Phys. **80**, 1625 (1984).

[58] E. Geva and R. Kosloff, A quantum-mechanical heat engine operating in finite time. A model consisting of spin-1/2 systems as the working fluid, J. Chem. Phys. **96**, 3054 (1992).

[59] T. Feldmann, E. Geva, R. Kosloff, and P. Salamon, Heat engines in finite time governed by master equations, Am. J. Phys. **64**, 485 (1996).

[60] M. Esposito, K. Lindenberg, and C. Van den Broeck, Universality of Efficiency at Maximum Power, Phys. Rev. Lett. **102**, 130602 (2009).

[61] Y. Rezek and R. Kosloff, Irreversible performance of a quantum harmonic heat engine, New J. Phys. **8**, 83 (2006).

[62] M. Esposito, R. Kawai, K. Lindenberg, and C. Van den Broeck, Efficiency at Maximum Power of Low-Dissipation Carnot Engines, Phys. Rev. Lett. **105**, 150603 (2010).

[63] S. Deffner, Efficiency of harmonic quantum Otto engines at maximal power, Entropy **20**, 875 (2018).

[64] R. Uzdin and R. Kosloff, Universal features in the efficiency at maximal work of hot quantum Otto engines, Europhys. Lett. **108**, 40001 (2014).

[65] O. Abah, J. Roßnagel, G. Jacob, S. Deffner, F. Schmidt-Kaler, K. Singer, and E. Lutz, Single-Ion Heat Engine at Maximum Power, Phys. Rev. Lett. **109**, 203006 (2012).

[66] X. L. Huang, D. Y. Guo, S. L. Wu, and X. X. Yi, Multilevel quantum Otto heat engines with identical particles, Quantum Inf. Process. **17**, 27 (2017).

[67] Y. Zheng and D. Poletti, Quantum statistics and the performance of engine cycles, Phys. Rev. E **92**, 012110 (2015).

[68] J. Jaramillo, M. Beau, and A. del Campo, Quantum supremacy of many-particle thermal machines, New J. Phys. **18**, 075019 (2016).

[69] K. Husimi, Miscellanea in elementary quantum mechanics, II, Prog. Theor. Phys. **9**, 381 (1953).

[70] E. Wigner, On the quantum correction for thermodynamic equilibrium, Phys. Rev. **40**, 749 (1932).

[71] Z. Gong, S. Deffner, and H. T. Quan, Interference of identical particles and the quantum work distribution, Phys. Rev. E **90**, 062121 (2014).

[72] F. Angulo-Brown, An ecological optimization criterion for finite-time heat engines, J. Appl. Phys. **69**, 7465 (1991).

[73] A. C. Hernández, A. Medina, J. M. M. Roco, J. A. White, and S. Velasco, Unified optimization criterion for energy converters, Phys. Rev. E **63**, 037102 (2001).

[74] P. Pietzonka and U. Seifert, Universal Trade-off Between Power, Efficiency, and Constancy in Steady-State Heat Engines, Phys. Rev. Lett. **120**, 190602 (2018).

[75] T. Yilmaz, A new performance criterion for heat engines: Efficient power, J. Energy Inst. **79**, 38 (2006).

[76] L. A. Arias-Hernandez, M. A. Barranco-Jiménez, and F. Angulo-Brown, Comparative analysis of two ecological type modes of performance for a simple energy converter, J. Energy Inst. **82**, 223 (2009).

[77] S. Velasco, J. M. Roco, A. Medina, J. White, and A. Hernéndez, Optimization of heat engines including the saving of natural resources and the reduction of thermal pollution, J. Phys. D: Appl. Phys. **33**, 355 (2000).

[78] V. Singh and R. S. Johal, Low-dissipation Carnot-like heat engines at maximum efficient power, Phys. Rev. E **98**, 062132 (2018).

[79] Y. H. Ma, D. Xu, H. Dong, and C. P. Sun, Universal constraint for efficiency and power of a low-dissipation heat engine, Phys. Rev. E **98**, 042112 (2018).

[80] S. Rana, P. S. Pal, A. Saha, and A. M. Jayannavar, Anomalous Brownian refrigerator, Physica A **444**, 783 (2016).

[81] S. Deffner and C. Jarzynski, Information Processing and the Second Law of Thermodynamics: An Inclusive, Hamiltonian Approach, Phys. Rev. X **3**, 041003 (2013).

[82] J. Bengtsson, M. N. Tengstrand, A. Wacker, P. Samuelsson, M. Ueda, H. Linke, and S. M. Reimann, Quantum Szilard Engine with Attractively Interacting Bosons, Phys. Rev. Lett. **120**, 100601 (2018).

[83] J. Bengtsson, M. N. Tengstrand, and S. M. Reimann, Bosonic Szilard engine assisted by Feshbach resonances, Phys. Rev. A **97**, 062128 (2018).

[84] A. Ronzani, B. Karimi, J. Senior, Y. C. Chang, J. T. Peltonen, C. Chen, and J. P. Pekola, Tunable photonic heat transport in a quantum heat valve, Nat. Phys. **14**, 991 (2018).

[85] J. J. Park, K. H. Kim, T. Sagawa, and S. W. Kim, Heat Engine Driven by Purely Quantum Information, Phys. Rev. Lett. **111**, 230402 (2013).

[86] A. Hewgill, A. Ferraro, and G. De Chiara, Quantum correlations and thermodynamic performances of two-qubit engines with local and common baths, Phys. Rev. A **98**, 042102 (2018).

[87] K. Micadei, J. P. S. Peterson, A. M. Souza, R. S. Sarthour, and I. S. Oliveira, Reversing the direction of heat flow using quantum correlations, Nat. Commun. **10**, 2456 (2019).

[88] O. Abah and M. Paternostro, Implications of non-Markovian dynamics on information-driven engine, arXiv:1902.06153.

[89] A. Levy, L. Diósi, and R. Kosloff, Quantum flywheel, Phys. Rev. A **93**, 052119 (2016).

[90] S. Toyabe, T. Sagawa, M. Ueda, E. Muneyuki, and M. Sano, Experimental demonstration of information-to-energy conversion and validation of the generalized Jarzynski equality, Nat. Phys. **6**, 988 (2010).

[91] K. Funo, Y. Watanabe, and M. Ueda, Thermodynamic work gain from entanglement, Phys. Rev. A **88**, 052319 (2013).

[92] S. W. Kim, T. Sagawa, S. De Liberato, and M. Ueda, Quantum Szilard Engine, Phys. Rev. Lett. **106**, 070401 (2011).

[93] M. Plesch, O. Dahlsten, J. Goold, and V. Vedral, Maxwell's daemon: Information versus particle statistics, Sci. Rep. **4**, 6995 (2014).

[94] H. T. Quan, Y. D. Wang, Y.-x. Liu, C. P. Sun, and F. Nori, Maxwell's Demon Assisted Thermodynamic Cycle in Superconducting Quantum Circuits, Phys. Rev. Lett. **97**, 180402 (2006).

[95] T. Busch, B. G. Englert, K. Rzażewski, and M. Wilkens, Two cold atoms in a harmonic trap, Found. Phys. **28**, 549 (1998).

[96] J. Goold, L. Heaney, T. Busch, and V. Vedral, Detection and engineering of spatial mode entanglement with ultracold bosons, Phys. Rev. A **80**, 022338 (2009).